NUMERICAL ANALYSIS OF AXISYMMETRIC TURBULENT SWIRLING FLOW IN CIRCULAR PIPE

by

Aleksandar S. ĆOĆIĆ*, Milan R. LEČIĆ, and Svetislav M. ČANTRAK
Faculty of Mechanical Engineering, University of Belgrade, Belgrade, Serbia

Original scientific paper
DOI: 10.2298TSCI130315064C

In this paper, turbulent swirling flow in circular pipe is numerically investigated using OpenFOAM, an open-source computational fluid dynamics software. Flow is computed as 2-D axisymmetric, with various turbulent models, but with main accent on computations with Reynolds stress transport models. Two Reynolds stress models were used in computations: Launder-Gibson and Speziale-Sarkar-Gatski models. Previous author's experimental results are used as a validation tool for numerical computations. It was shown that standard two-equation models can not predict the flow in right manner, while the Reynolds stress models give good prediction of mean velocities. As a part of research Speziale-Sarkar-Gatski model is implemented in OpenFOAM code.

Key words: *swirling flow, OpenFOAM, turbulence modeling*

Introduction

Turbulent swirling flows are very present flow phenomena in various technical applications such as turbomachinery, large pipeline systems, cyclone separators, combustion chambers, *etc*. In some applications swirl is intentionally generated, in order to improve the performance of the device. In centrifugal separators, swirl is the major factor that leads to separation of particle due to centrifugal forces. In combustors swirl significantly contribute in faster mixing of the reacting components during burning process. It was also noted that it creates re-circulation zones where the temperature of species is maintained sufficiently high for a long period of time. On the other hand, swirl is sometimes regarded as the unwanted phenomena. In usually in the cases of sudden geometry changes or unexpected flow conditions.

Swirling flows can be viewed as combination of vortex flow and axial velocity, which causes fluid to move in helicoidal trajectories, where the velocities vary mainly in respect to axial and radial co-ordinate. This is strongly depended on the way how the swirl is generated, but it's quite common that swirl can be regarded as axisymmetric. Turbulence structure in swirling flow is highly anisotropic as a consequence of additional flow phenomena that are not present in simple shear flow, like shear component $\partial W/\partial r$, in addition to common mean shear $\partial U/\partial r$ and streamline curvature. All these phenomena are the reasons why standard turbulent models based on linear eddyviscosity in most cases of swirling flows gives uncorrect prediction of the flow.

* Corresponding author; e-mail: acocic@mas.bg.ac.rs

Because of their practical and theoretical importance swirling flows have been extensively studied in past few decades. Most of the studies were focused on internal swirling flow, particularly on flow in the pipes. Some of experimental results of swirling flow in pipes are given in [1-14].

As pointed out in [15], due to physical phenomena that are present, modeling of swirl flows is still perpetual challenge. In [16] authors showed that nor k-ε model nor it's modifications with higher order terms are not capable to predict the axial and tangential velocity profiles in swirl flow because the eddy viscosity components are anisotropic. They proposed a modified k-ε model which considered an anisotropic factor for eddy viscosity, which was much more successful in prediction of mean velocity profiles. It was also found in [17] that k-ε model is not successful in solving the velocity field in swirling flows. On the other hand, in [18] it was proved both experimentally and numerically, in case of weak swirling flows standard k-ε model can successfully predict the flow. Numerical investigations in [19] showed that for low swirl, RNG k-ε model gives better prediction than Reynolds stress model, while for higher swirl, Reynolds stress models are more appropriate. In [19] so called "solid-body" swirl is modeled, where in most part of pipe cross-section, except the wall region, fluid rotates with constant angular velocity. In that cases, k-ε model and other two-equation models based on isotropic-eddy viscosity can have good performances, because their formulation always gives "solid-body rotation" form of tangential velocity profile, independent of velocity profile given at the inlet [15].

In this paper, numerical simulation of swirling flow in the pipe with Rankine vortex profile for tangential velocity for different values of swirl number is performed using various turbulence models.

Problem is considered as axisymmetric and it was shown that two equation models gives poor prediction for both axial and tangential velocity, for each value of swirl number. On the other hand, second-order closures, *i. e*. Reynolds stress models, Launder and Gibson (LG) [20] and Speziale Sarkar Gatski (SSG) model, [21] give very good results. SSG model showed better performances for higher values of swirl number. For all numerical simulation open--source computational fluid dynamics (CFD) software OpenFOAM was used. Thanks to fact that code is open, during this research the SSG model was implemented in the OpenFOAM code.

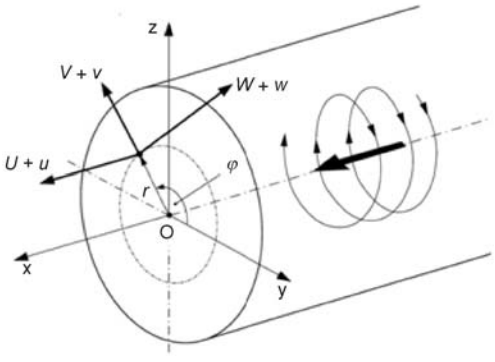

Figure 1. Co-ordinate system and velocities in turbulent swirling flow in the pipe

Characteristics of internal swirl flows

Because of the nature of swirling flow and the fact that this type of flow is mostly present in circular geometries, it is natural to adopt cylindrical co-ordinate system (x, r, φ) for its description, and to define velocities components accordingly, which is shown in fig. 1.

Velocity components are represented as the sum of mean (time-averaged) and fluctuating velocity, as defined with Reynolds statistical description of turbulent flow. Mean axial velocity is designated with U, while V and W represent mean radial and tangential (circumferential) velocity, respectively. Fluctuating velocities are u, v, and w, which are axial, radial

and circumferential velocity fluctuations, respectively. There are several different methods for generation of swirling flow in circular pipes [22]. In most cases, radial velocity is much smaller in comparison to axial and tangential ones, and it usually can be neglected, [1, 9]. The most important component is definitely circumferential component, and its distribution is directly related to the way how the swirl is generated.

A suitable measure for amount of swirl is swirl number, which is usually defined as the ratio of angular and linear momentum, which in case of axisymmetric flow fields have the form:

$$S = \frac{\int_0^R r^2 UW \mathrm{d}r}{R\int_0^R rU^2 \mathrm{d}r} \tag{1}$$

where R is the pipe radius. Another definition which can be found in literature, for example in [10], takes the flux of linear momentum based on bulk velocity $U_m = V/(R^2\pi)$. In that case swirl number is defined as:

$$S = \int_0^1 \left(\frac{r}{R}\right)^2 \frac{U}{U_m}\frac{W}{U_m} d\left(\frac{r}{R}\right) \tag{2}$$

Other authors, Čantrak [3], as a measure of amount of swirl use swirl intensity, defined as:

$$\theta_p = \frac{\int_0^R rW^2 U \mathrm{d}r}{\int_0^R rU^3 \mathrm{d}r} \tag{3}$$

Both swirl number and swirl intensity are integral characteristics of flow field, and it is worth mentioning that different types of swirl flows can have the same swirl number. But high values of swirl number is usually connected with high intensity of tangential velocity. Recent theoretical and experimental studies on helical vortex structures in swirl flows given in [23] showed that under the same integral flow parameters (flow rate, flow circulation, swirl and Reynolds number) that both left-handed and right handed vortex-structures can be realized, and in that sense they showed that swirl number is not sufficient parameter which can be used to completely describe this type of flows.

In the case of Rankine vortex profile for tangential velocity three regions with different physics can be distinguished: core, annular and wall region. In the core region, characterized by a solid body rotation, the turbulence intensity is stabilized ensuring a favorable radial pressure gradient distribution whereas in annular region, turbulence intensity may be destabilized due to formation of free vortex profile. In addition, the skewness of the velocity vector in annular region is noticeable and highly anisotropic. In wall region the flow can be viewed as boundary-layer type of flow. Due to the dissipation effects the intensities of circumferential velocity and swirl number are decreasing in the direction of the flow, *i. e*. in downstream cross-sections. This phenomena is known as swirl decay, and in most references [1, 9, 10], it is described with exponential decay function:

$$S = \alpha \exp\left(-\frac{\beta x}{R}\right) \tag{4}$$

where α and β are constants, and x is the co-ordinate directed along the pipe axis. In decay process, the shape of the profile for both axial and circumferential velocity is changing. In the case

of high swirl, axial velocity can even have a back-flow in the core region, which is gradually vanish in downstream sections with decrease of swirl, and the U profile is slowly transforming in fully developed axial flow profile.

Experimental database

In this research, experimental results of Čantrak [3] were used as validation tool for numerical computations. The sketch of experimental rig is given in fig. 2. The working medium was air, and the measuring technique was hot-wire anemometry. The swirl is generated with stationary blades, which are deflecting the flow to characteristic helicoidal shape, and generate the circumferential velocity. This way of swirl generation produces Rankine vortex profile for circumferential velocity. By adjusting the angle of the blades, intensity of the swirl can also be adjusted. There were seven measuring sections in the pipe, and three different blade angles: $\alpha = 15°$, 30°, and 45°. For these values of the blade angles the corresponding values of swirl intensities, defined with eq. (3), and calculated with velocities in first measuring section were $\theta_p = 0.229$, 0.385, and 0.429, respectively. Bulk velocity in all three cases was $U_m = 21.41$ m/s, and pipe diameter $D = 200$ mm. Reynolds number based on these two parameters was $\mathrm{Re} = 2.835 \cdot 10^5$. First measuring section was at the distance $L = 350$ mm from the pipe entrance, and that section is designed as $x = 0$. Measuring data from that section was used as the inlet data in numerical simulations.

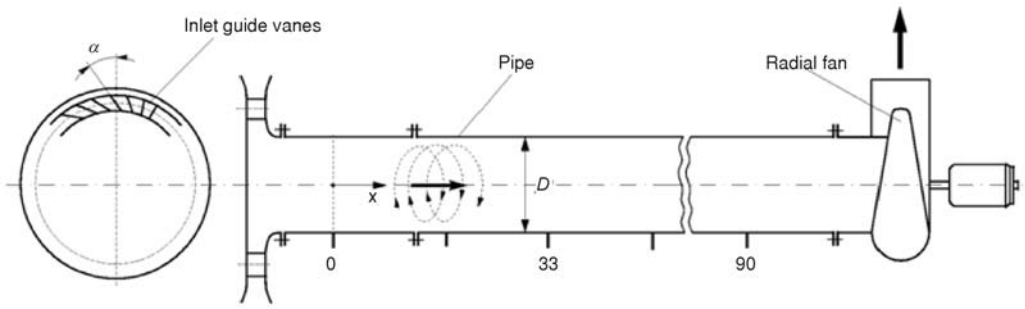

Figure 2. Sketch of experimental installation used in experimental investigation of swirl flows in [3]

Governing equations

In contrast to the transport equations for Reynolds stresses and Reynolds stress closures which are usually written using index notation, all the equations in this paper are written in invariant form, *i. e*. all physical quantities are represented as objects. There are two reasons for that. Firstly, that type of equation representing is independent of the choice of co-ordinate system, and characteristics terms that appear in fundamental equations of fluid mechanics, like diffusion, convection and source terms are easily recognized. The second, and more important reason is directly related to high level of abstraction used in design and programming of OpenFOAM code, where physical quantities are viewed as tensors up to rank 2. Implementation of numerical algorithms used for solving partial differential equations in such programming environment is very much based on invariant form of the equations.

The flow of incompressible, Newtonian fluid is described by fundamental principles of conservation of mass and momentum. From those fundamental principles continuity and Navier-Stokes equations are obtained. In case of turbulent flows, where there is a broad range of

time and spatial scales, solution of Navier-Stokes equation is possible to obtain only by direct numerical simulation (DNS), for relatively small values of Reynolds numbers and in simple geometries. In past few years, with rapid and strong development of computing power, large eddy simulation (LES) are more and more applicable for numerical computations of fluid flow. But still, for analysis of engineering problems, Reynolds averaged Navier-Stokes (RANS) aproach is still the best compromise between accuracy and computational resources (and time) needed for calculation.

Applying the Reynolds statistics on continuity and momentum equation, their time-averaged form is obtained. Written in so-called "strong-conservative" form, they are:

$$\nabla\vec{\mathrm{U}} = 0 \tag{5}$$

$$\frac{\partial\vec{\mathrm{U}}}{\partial t} + \nabla(\vec{\mathrm{U}}\vec{\mathrm{U}}) = -\nabla P^* + \nabla(\nu\nabla\vec{\mathrm{U}} - \overline{\vec{\mathrm{u}}\vec{\mathrm{u}}}) \tag{6}$$

where $\vec{\mathrm{U}}$ is the time averaged velocity vector, $P^* = P/\rho$ – the time averaged kinematic pressure, ν – the kinematic viscosity, and $\mathbf{R} = \overline{\vec{\mathrm{u}}\vec{\mathrm{u}}} \equiv \overline{\vec{\mathrm{u}} \otimes \vec{\mathrm{u}}}$ is the Reynolds stress tensor, written in it's dyadic form.

Reynolds stress modeling

Reynolds stress closures involves additional six equations for components $\overline{u_i u_j}$ of tensor **R**, plus one equation for turbulence energy dissipation ε, in order to close the system of eqs. (5) and (6).

The general form of Reynolds stress closure can be written as:

$$\partial_{\mathrm{t}}\,\mathbf{R} + \vec{\mathrm{U}}\nabla\mathbf{R} = \mathbf{P} - \mathbf{E} + \mathbf{D} + \mathbf{F} \tag{7}$$

where **P**, **D**, **F**, and **E** are second order tensors which represents production, diffusion, redistribution, and dissipation, respectively. Production term represents the generation of Reynolds stresses by interaction between the stress and mean strain:

$$\mathbf{P} = -[\mathbf{R}(\nabla\vec{\mathrm{U}}) + (\nabla\vec{\mathrm{U}})^T\,\mathbf{R}] \tag{8}$$

This term is exact, it is obtained from derivation of the transport equation for Reynolds stresses, and there is no need to be modeled.

For high Reynolds number flows, Kolmogorov hypothesis of local isotropy is more pronounced and it is used for modeling the tensor of dissipation:

$$\mathbf{E} = \frac{2}{3}\varepsilon\mathbf{I} \tag{9}$$

where ε is the (scalar) turbulent dissipation rate, and **I** is the unit tensor.

Diffusion term can be modeled in two ways, by simplified gradient-diffusion model, or by general, non-isotropic form. In this paper, general form for diffusion term was used:

$$\mathbf{D} = \nabla\left[\nu\nabla\mathbf{R} + C_{\mathrm{s}}\frac{k}{\varepsilon}\mathbf{R}\nabla\mathbf{R}\right], \quad k = \frac{1}{2}\mathrm{tr}[\mathbf{R}] \tag{10}$$

where $C_{\mathrm{s}} = 0.22$ is the model constant, k – the turbulent kinetic energy, while ε – the turbulent dissipation rate. In most cases, linear molecular diffusion part term is much smaller in comparison to the non-linear part and is often neglected.

The rate of turbulence energy dissipation which appears in eq. (7) is determined from its transport equation, which in case of second-order closures takes the form:

$$\frac{\partial \varepsilon}{\partial t} + \vec{\mathrm{U}}\nabla\varepsilon = C_{\varepsilon 1}\frac{\varepsilon}{k}P_k + \nabla\left[C_\varepsilon \frac{k}{\varepsilon}\mathbf{R}\nabla\varepsilon\right] - C_{\varepsilon 2}\frac{\varepsilon^2}{k} \tag{11}$$

where $P_\mathrm{k} = (1/2)\mathrm{tr}(\mathbf{P})$ turbulence kinetic energy production, while C_ε, $C_{\varepsilon 1}$, and $C_{\varepsilon 2}$ are constants, which are 0.15, 1.44, and 1.92, respectively. In comparison to the ε equation in k-ε model, turbulent diffusion term in eq. (11) is anisotropic.

Modeling of redistribution, or pressure-strain term is perpetual challenge in Reynolds stress closures. In this paper, two different approaches were tested on the case of swirling pipe flow. In first approach, suggested in Launder-Gibson model [20] redistribution term is modeled by linear function of Reynolds stress. It is usually represented as sum of three tensors, $\mathbf{F} = \mathbf{F}_1 + \mathbf{F}_2 + \mathbf{F}_\mathrm{w}$, where the individual terms are defined as:

$$\mathbf{F}_1 = -1.8\frac{k}{\varepsilon}\left[\mathbf{R} - \frac{1}{3}\mathrm{tr}(\mathbf{R})\mathbf{I}\right] \tag{12}$$

$$\mathbf{F}_2 = -0.6\frac{k}{\varepsilon}\left[\mathbf{P} - \frac{1}{3}\mathrm{tr}(\mathbf{P})\mathbf{I}\right] \tag{13}$$

$$\begin{aligned}\mathbf{F}_\mathrm{w} = {} & 0.5\frac{\varepsilon}{k}\{[\mathbf{R}:(\vec{\mathrm{n}}\otimes\vec{\mathrm{n}})]\mathbf{I} - 1.5[\vec{\mathrm{n}}\otimes(\mathbf{R}\vec{\mathrm{n}}) + (\vec{\mathrm{n}}\mathbf{R})\otimes\vec{\mathrm{n}}]\}f + \\ & + 0.3\{[\mathbf{F}_2:(\vec{\mathrm{n}}\otimes\vec{\mathrm{n}})]\mathbf{I} - 1.5[\vec{\mathrm{n}}\otimes(\mathbf{F}_2\vec{\mathrm{n}}) + (\vec{\mathrm{n}}\mathbf{F}_2)\otimes\vec{\mathrm{n}}]\}f\end{aligned} \tag{14}$$

where $\vec{\mathrm{n}}$ is the wall unit normal vector and $f = C_\mu^{0.75}\kappa^{1.5}/(\varepsilon\kappa y)$ with y being the distance from the closest wall along the coordinate line normal to the wall. Constants C_μ and κ are equal to 0.09 and 0.41, respectively. Term $\mathbf{F}_\mathrm{w}$ is so-called wall reflection term and it is taking into account that proximity of a rigid wall modifies the pressure field, thus impeding the transfer of energy from the streamwise direction to direction normal to the wall [20].

Instead of linear dependence for pressure-strain term, alternative non-linear dependence obtained with invariant dynamical approach is suggested in [21]. In this approach, pressure-strain tensor is defined as the sum of tensors $\mathbf{F}_1$ and $\mathbf{F}_2$, defined as:

$$\mathbf{F}_1 = -(C_1\varepsilon + C_1^* P_\mathrm{k})\mathbf{B} + C_2\varepsilon\mathrm{dev}[\mathbf{BB}] \tag{15}$$

$$\mathbf{F}_2 = (C_3 - C_3^*\sqrt{II_B})k\mathbf{S} + C_4 k\left[\mathbf{BS} + \mathbf{SB} - \frac{2}{3}(\mathbf{B}:\mathbf{S})\mathbf{I}\right] + C_5 k(\mathbf{WB} + \mathbf{BW}^T) \tag{16}$$

where

$$P_k = \frac{1}{2}\mathrm{tr}(\mathbf{P}), \quad \mathbf{B} = \frac{1}{2k}\mathbf{R} - \frac{1}{3}I, \quad II_\mathrm{B} = \mathbf{B}:\mathbf{B}, \quad \mathbf{S} = \frac{1}{2}[(\nabla\vec{\mathrm{U}})^T + \nabla\vec{\mathrm{U}}], \quad \mathbf{W} = \frac{1}{2}[(\nabla\vec{\mathrm{U}})^T - \nabla\vec{\mathrm{U}}]$$

which are production, normalized anisotropy tensor, second invariant of anisotropy tensor, and vorticity tensor, respectively. In contrast to Launder-Gibson model, this model does not have wall reflection term. Constants of the model are given in tab. 1.

Table 1. Constants in Speziale-Sarkar-Gatski (SSG) model

C_1	C_1^*	C_2	C_3	C_3^*	C_4	C_5
3.4	1.8	4.2	0.8	1.3	1.25	0.40

Results of numerical simulations

Implementation of SSG model in OpenFOAM

OpenFOAM is well-tested and widely used open-source CFD software. It is written in C++, and it is essentially a collection of libraries which are primarily used to create various applications. OpenFOAM is distributed with a large set of precompiled applications, but due to the fact that the code is open, users can create their own applications and solvers or modify the existing ones.

Regarding the turbulence modeling, there are dozen of RAS models implemented in OpenFOAM – including standard, non-linear, low-Re number models and from group of second order closures, Launder-Reece-Rodi (LRR) and Launder-Gibson Reynolds stress models. OpenFOAM is designed mainly as a research tool, and all turbulence models are implemented in the code as a set of classes with a common interface [24]. This common interface is defined via base class named turbulenceModel, and various RAS models are defined by other classes derived from the base class, which is the great advantage and one of the characteristics of C++ programming language – inheritance. That facts make the implementation of the new model in the code, besides some additional work on proper linking and definition of constants, more or less straightforward – by following the equations of the model written in their invariant form.

A part of the code where deformation rate and vorticity are calculated is given in the following lines:

```
volTensorField nablaU = fvc::grad(U_);          // velocity gradient tensor
volSymmTensorField S = symm(nablaU);            // deformation rate tensor
volTensorField W = skew(nablaU.T());            // vorticity tensor
volSymmTensorField B = dev(R_)/tr(R_);          // anisotropy tensor
```

A class designed as fvc:: defines explicit calculation of velocity gradient tensor from the known velocity field in each time step during computation.

Formation of linear matrix which corresponds to Reynolds stress equation is given in the following lines:

```
tmp<fvSymmTensorMatrix> REqn
(
    fvm::ddt(R_)
    + fvm::div(phi_, R_)
    + fvm::SuSp(-fvc::div(phi_), R_)
    - fvm::laplacian(Cs_*(k_/epsilon_)*R_, R_)
    + fvm::Sp(Cssg1_*epsilon_/(2*k_), R_)
    + fvm::Sp(Cssg1Ast_*Pk/(2*k_), R_)
  ==
    P - 2.0/3.0*epsilon_*I
    + 1.0/3.0*(Cssg1_*epsilon_ + Cssg1Ast_*Pk)*I
    + Cssg2_*epsilon_*dev(B & B)
    + (Cssg3_ - Cssg3Ast_*mag(B))*k_*S
    + Cssg4_*k_*(twoSymm(B & S) - 2.0/3.0*(B && S)*I)
    + Cssg5_*k_*twoSymm(B & W.T())
);
```

It can be seen that representation of the code mimics the mathematical equation, written in it's invariant form, *via* physical objects. Class fvm:: means that those terms are treated im-

plicitly. Other terms are treated in explicit way and they are calculated in previous iteration, or previous time step. Discretization schemes for implicit terms are defined in separate file, in terminology of OpenFOAM known as dictionary file. In implementation of the pressure-strain term in the code linear parts are added in the implicit part of source term in Reynolds stress equation, by which diagonal dominance of R-matrix is increased. Increased diagonal dominance can significantly improve the stability of the computation.

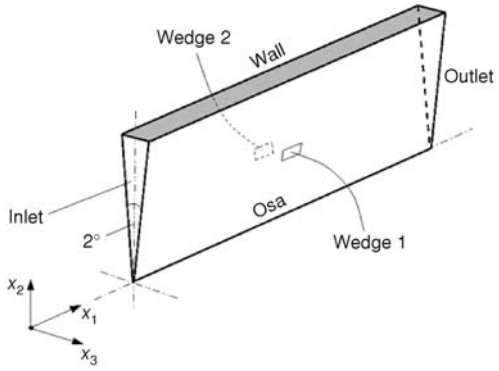

Figure 3. Computational domain

Numerical set-up in OpenFOAM

Because the problem was considered as axisymmetric, the computational domain was specified as a wedge of small angle (<5°), and one cell thick running along the plane of symmetry, as explained in [25], and shown in fig. 3. The length of the domain was 10 meters, while height of the wedge was equal to the pipe radius, which was 0.1 meter. Due to the simplicity of the domain, OpenFOAM mesh generator blockMesh was used for generation of block-structured grid. For grid independence test, three different meshes were created, with 400 × 30, 600 × 40, and 800 × 60 cells in axial and radial direction, respectively. Non-uniform grading was used in both directions; cells are stretched in axial direction, while in radial direction cells are compressed both near the wall and near the pipe axis.

The height of first cell near the wall was chosen to be 1 mm for each mesh, which gave the mean value of $y^+ \approx 30$ in all cases. That is because both LG and SSG models are formulated in so-called high-Re approach, *i. e*. they are using wall functions. It means that law of the wall is used to bridge the viscous sublayer, and the nearest computational point (cell center) to the wall is in logarithmic region.

At the inlet, experimental values of mean velocities and turbulent stresses from the first measuring sections are prescribed, and zero gradient for pressure. On the lateral surfaces, boundary condition called wedge was used, for every variable. This boundary condition imposes equal fluxes on lateral sides, but with opposite signs. At the outlet zero gradients for velocities and turbulent stresses was used, while for the pressure fixed mean value boundary condition was used. This boundary condition allows that pressure varies on the surface, with some prescribed mean value. Because the flow is assumed as incompressible, zero mean value for the pressure was chosen at the outlet.

Velocity-pressure coupling was accomplished by segregated methods, in which continuity equation is used to formulate equation for pressure, using a semi-discrete momentum equation. The resulting equation set is solved by a decoupled approach, using iterative algorithms. For computation both steady and unsteady solvers were used. In the first case, for pressure-velocity coupling SIMPLE algorithm with under-relaxation was used, while for unsteady computations, PISO algorithm was used [26, 27]. For higher values of swirl intensity for both models unsteady approach was used, because with steady solver it was impossible to get the solution convergence, by which is confirmed that time marching can improve stability, which is in agreement with research presented in [28].

Results and discussion

First, the results of simulation with two equations models are given. Both high-Re and low-Re models were used. For low-Re formulation a different mesh was used, with more cells in radial direction. The distance from the wall to the center of closest cell was 0.01 mm, chosen to ensure $y^+ \approx 1$. Each case was computed as a steady, and it took in average 8000 outer iterations for high-Re models and 30000 outer iterations for Launder-Sharma low-Re model to get converged solution. Basically, there were no significant difference in predicted results for both group of models. They were all, more or less, completely wrong, specially for the highest values of swirl intensities and specially for circumferential velocity. Here only the results for the weakest swirl are shown, where the discrepancies are the smallest, but still quite significant, fig. 4. It can be seen that every model predict too soon fully developed profile for axial velocity, while for circumferential velocity they predict completely wrong type of profile, a "solid-body". The differences in experimental and numerical results for other, higher values of swirl intensities are more pronounced, specially in the core region, where the low values of axial velocity are present.

These kind of failures of two-equation models, based on linear, scalar eddy viscosity assumptions are not present in Reynolds stress closures. But still, there are also significant differences in results for axial velocity in the core in case of strong swirls between the results of two models used in this research. Launder-Gibson (LG) model showed as more robust, and it was possible to compute the flow with steady solver, by taking smaller values of under-relaxation

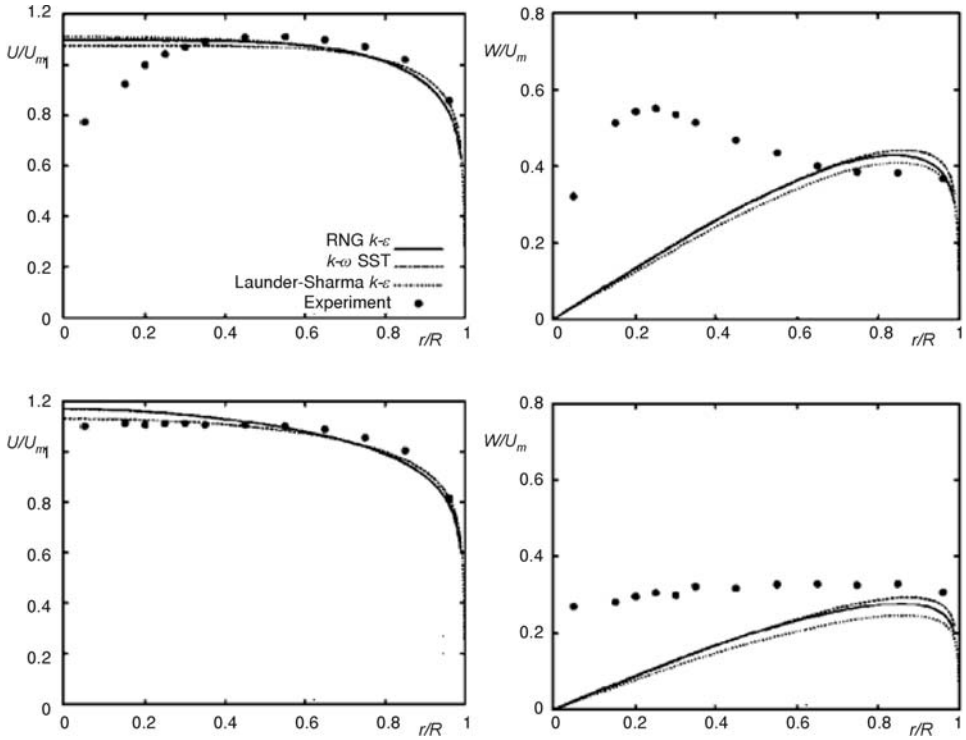

Figure 4. Profiles of mean velocities *U* and *W* obtained with two-equation models for swirl intensity $\theta_p = 0.229$. First line: measuring section *x/R* = 33, second line: measuring section *x/R* = 90

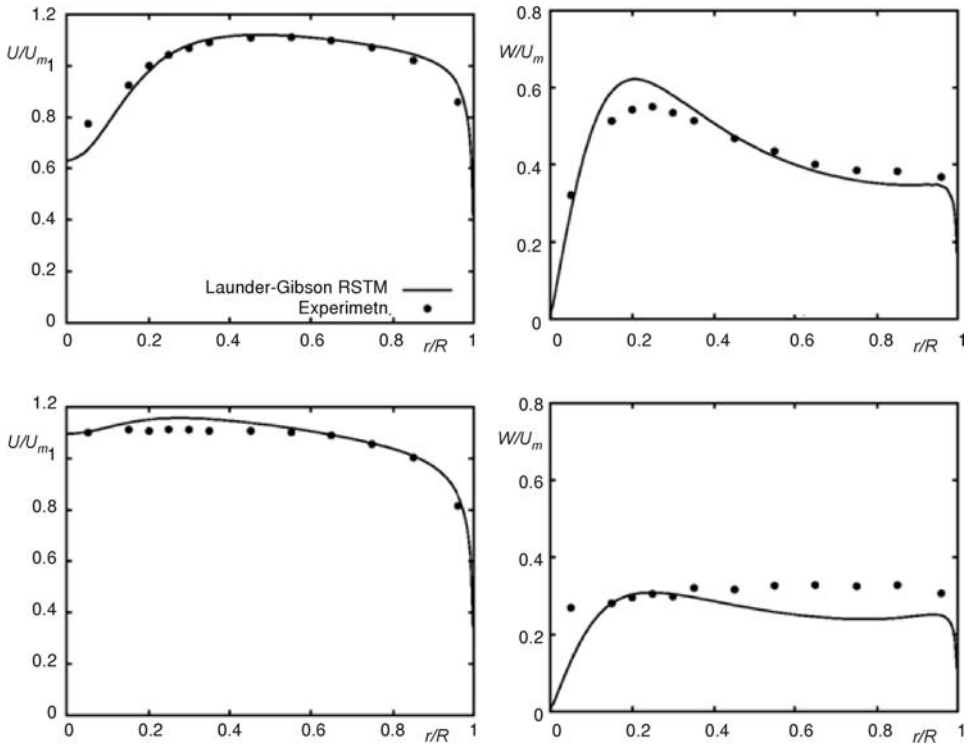

Figure 5. Profiles of mean velocities *U* and *W* for $\theta_p = 0.229$. First line: measuring section *x/R* = 33, second line: measuring section *x/R* = 90

factors for turbulence quantities. In case of implemented SSG model stability of computation is enhanced with time-marching, and use of unsteady solver.

For steady computation with LG model, it took 50000 outer iterations to achieve converged solution, while in unsteady simulations it took about $2 \cdot 10^5$ iterations to reach steady-state solution. For the lowest version of swirl intensity, $\theta_p = 0.229$ the region of low axial velocity in core region is not so pronounced and prediction of mean velocities are in very good agreement with experimental results, which is shown in fig. 5. The results obtained with SSG model in this case are quite similar.

For higher values of swirl intensity mean axial velocity in the core region is decreasing, and the LG model predicts too diffusive profile in this region, while the SSG model captures well this behavior in that region, fig. 6.

For higher values of swirl, interesting behavior in prediction of circumferential velocity with SSG model was found in regions near the wall, where small oscillations in profile are present. These oscillations are more pronounced near the inlet, and they are decreasing in axial direction (and vanishing approximately at *x/R* = 50). One of the possible reason for is radial velocity profile in first measuring section, where a sudden change in its sign is present in last measuring point. These profiles are shown in fig. 7. In these experiments, radial velocity was in range 4-10% of bulk velocity.

The high gradient of radial velocity between the last two measuring points, together with the fact that from the last measuring point velocity goes to zero, which is another high gra-

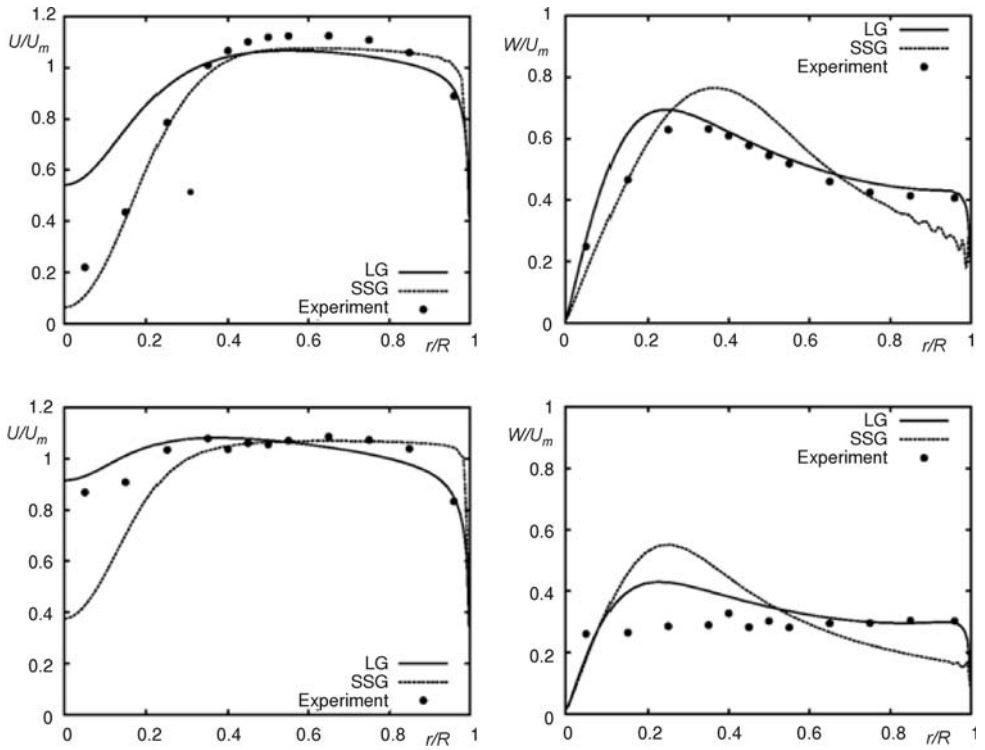

Figure 6. Profiles of mean velocity for swirl intensity θ_p = 0.429. First line: measuring section *x/R* = 33, second line: measuring section *x/R* = 90

dient and presence of inflection point clearly shows that use of wall functions is debatable in this case. It is suspected that this zig-zag behaviour of radial velocity near the wall is the main reason for similar behavior of circumferential velocity, predicted by models. Also, this effect is more pronounced in case of SSG model. One of the explanation for that could in the fact the LG model has wall-reflection term, while SSG model has not. Further tests using different experimental databases and modification of SSG model will hopefully give new insights in this interesting phenomena.

Both models give unsatisfactory prediction of Reynolds stresses, and they can not capture the higher values of normal turbulent stresses in core region. The main reason for that lies in fact that in reality the core is making precession movement, which is three dimensional and unsteady. In that sense, this kind of movement can only be predicted in 3-D computational domains, and with LES approach. With unsteady RANS in 3-D, and with constant velocities and turbulent stresses (axisymmetrically distributed) at the inlet, all un-

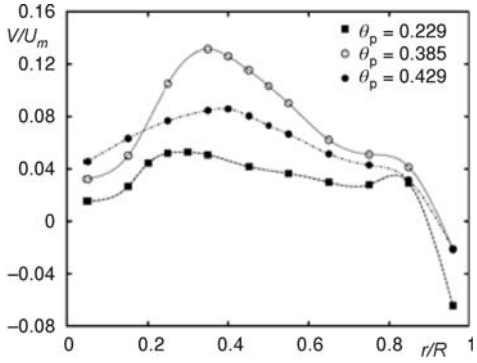

Figure 7. Measured profiles of radial velocity at position *x* = 0 (inlet section in numerical simulation)

steadiness will be damped and one will get the steady solution, similar to computations from 2-D simulations.

Conclusions

In this paper turbulent swirling flow in circular pipe with Rankine profile for circumferential velocity was numerically computed using the OpenFOAM software. Computations were performed under assumption of axisymmetric flow. It was shown that standard, two-equation turbulent models are enable to capture characteristic behaviour of mean velocities in this type of flow. Second order closures, or Reynolds stress transport models give better prediction of mean flow characteristics. Two Reynolds stress models were tested in this research – Launder-Gibson (LG) and Speziale-Sarkar-Gatski (SSG). The main difference between these two models are in their formulation of pressure-strain term. Both models predict the mean flow quite well, specially in the case of weak swirl. In cases of strong swirl, LG model is over-diffusive in the core region and predicts too high values of axial velocity, while SSG model gives better agreement with experimental results. In case of circumferential velocity, for higher values of swirl intensity SSG model predicts higher values than LG model, and in general higher intensity of circumferential velocity than obtained by experiments. Current and future research will be dedicated to computation of swirl flows with second-order closure with elliptic blending and without use of wall functions, based on model proposed in [29] and unsteady computations of swirl flows with axial fan as swirl generator.

Acknowledgment

This work is supported by the Ministry of Education, Science and Technological Development of the Republic of Serbia, project no. TR-35046, which we gratefully acknowledge.

Nomenclature

B – normalized anisotropy tensor, [–]
II_B – second invariant of anisotropy tensor, [–]
D – diffusion tensor, [m^2s^{-3}]
E – specific dissipation tensor, [m^2s^{-3}]
F – redistribution tensor, [m^2s^{-3}]
k – turbulence kinetic energy, [m^2s^{-2}]
P – production tensor, [m^2s^{-3}]
P^* – averaged kinematic pressure, [m^2s^{-2}]
P_k – production of k, [m^2s^{-3}]
R – Reynolds stress tensor, [m^2s^{-2}]
S – mean shear rate tensor, [s^{-1}]
S – swirl number, [–]
U – mean axial velocity, [ms^{-1}]
$\bar{U}$ – time averaged velocity vector, [ms^{-1}]
u – fluctuation of axial velocity, [ms^{-1}]
V – mean radial velocity, [ms^{-1}]
v – fluctuation of radial velocity, [ms^{-1}]
W – mean vorticity tensor, [s^{-1}]
W – mean tangential velocity, [ms^{-1}]
w – fluctuation of tangential velocity, [ms^{-1}]

Greek symbols

ε – specific dissipation rate, [m^2s^{-3}]
ν – kinematic viscosity, [m^2s^{-2}]
θ_p – swirl intensity, [–]

References

[1] Benišek, M.H., Investigation of the Swirl Flow in Pipes, Ph. D. thesis, Faculty of Mechanical Engineering, University of Belgrade, Belgrade, Serbia, 1979
[2] Lečić, M. R., Theoretical and Experimental Investigation of Turbulent Swirling Flows, Ph. D. thesis, Faculty of Mechanical Engineering, University of Belgrade, Belgrade, 2003
[3] Čantrak, S.M., Experimental Investigation of the Statistical Properties of Swirling Flows in Pipes and Diffusers, Ph. D. thesis, Karlsruhe University, Karlsruhe, Germany, 1981
[4] Benišek, M., *et al*., Application of New Classic Probes in Swirl Fluid Flow Measurements, *Experimental Techniques, 34* (2010), 3, pp 74-81

[5] Vukašinović, B., Turbulent Transport Processes and Problems in its Modeling in Swirl Flows, M. Sc. thesis, Faculty of Mechanical Engineering, University of Belgrade, Belgrade, 2003
[6] Čantrak, Dj., Analysis of the Vortex Core and Turbulence Structure behind Axial Fans in a Straight Pipe Using PIV, LDA and HWA Methods, Ph. D. thesis, Faculty of Mechanical Engineering, University of Belgrade, Belgrade, 2012
[7] Lečić, M., *et al.*, Original Measuring and Calibration Equipment for Investigation of Turbulent Swirling Flow in Circular Pipe, Experimental Techniques, Accepted for Printing, Article First Published Online 14. Feb. 2012, DOI: 10.1111/j.1747-1567.2012.00812.x
[8] Kreith, F., Sonju, K., The Decay of Turbulent Swirl Flow in a Pipe, *Journal of Fluid Mechanics, 22* (1965), 2, pp. 257-271
[9] Kitoh, O., Experimental Study of Turbulent Swirling Flow in a Straight Pipe, *Journal of Fluid Mechanics, 225* (1991), pp. 445-479
[10] Steenbergen, W., Turbulent Pipe Flow with Swirl, Ph. D. thesis, Eindhoven University, The Netherlands,1995
[11] Rocklage-Marliani, G., *et al*., Three-Dimensional Laser-Doppler Velocimeter Measurements in Swirling Turbulent Pipe Flow, Flow, *Turbulence and Combustion, 70* (2003), 1-4, pp. 43-67
[12] Cazan, R., Aidun, C. K., Experimental Investigation of Swirling Flow and the Helical Vortices Induced by a Twisted Tape Inside a Circular Pipe, *Physics of Fluids, 21* (2009), 3, pp. 102-109
[13] Ho, K., *et al*., An Experimental Set-Up for Investigating Swirling Decaying Flow in an Annular Pipe, *International Communications in Heat and Mass Transfer, 38* (2011), 9, pp. 1253-1261
[14] Ahmadvand, M., *et al*., An Experimental Study and CFD Analysis Towards Heat Transfer and Fluid Flow Characteristics of Decaying Swirl Pipe Flow Generated by Axial Vanes, *Meccanica, 45* (2010), pp. 111-129
[15] Jakirlić, S., Hanjalić, K., Tropea, C., Modeling Rotating and Swirling Turbulent Flows: A Perpetual Challenge, *AIAA Journal, 40* (2002), 10, pp. 1984-1996
[16] Kobayashi, T., Yoda, M., Modified k-ε Model for Turbulent Swirling Flow in a Straight Pipe, *JSME International Journal*, Series 2: Fluids Engineering, Heat Transfer, Power Combustion, *Thermophysical Properties, 259* (1987), 30, pp. 66-71
[17] Nejad, A. S., *et al*., Application of Laser Velocimetry for Characterization of Confined Swirling Flow, *Journal of Engineering for Gas Turbines and Power, 111* (1989), 1, pp. 36-45
[18] Bali, T., Ayhan, T., Experimental Investigation of Propeller Type Swirl Generator for a Circular Pipe Flow, *International Communications in Heat and Mass Transfer, 26* (1999), 1, pp. 13-22
[19] Escue, A., Cui, J., Comparison of Turbulence Models in Simulating Swirling Pipe Flows, *Applied Mathematical Modeling, 34* (2010), 10, pp. 2840-2849
[20] Gibson, M. M., Launder, B. E., Ground Effects on Pressure Fluctuations in the Atmospheric Boundary Layer, *Journal of Fluid Mechanics, 86* (1978), 3, pp. 491-511
[21] Speziale, C. G., *et al*., Modeling the Pressure-Strain Correlation of Turbulence: an Invariant Dynamical Approach, *Journal of Fluid Mechanics, 227* (1991), pp. 245-272
[22] Gupta, A. K., *et al*., *Swirl Flows, Energy and Engineering Sciences Series*, Abacus Press, UK, 1984
[23] Alekseenko, S. V., *et al*., Helical Vortices in Swirl Flow, *Journal of Fluid Mechanics, 382* (1999), pp. 195-243
[24] Weller, H. G., *et al*., A Tensorial Approach to CFD using Object Orientated Techniques, *Computers in Physics, 12* (1998), 6, pp. 620-631
[25] ***, OpenCFD Ltd. OpenFOAM User Guide, Version 1.6, July 2007
[26] Patankar, S. V., Spalding, D. B., A Calculation Procedure for Heat, Mass and Momentum Transfer in Three-Dimensional Parabolic Flows, *Int. Heat Mass Transf., 115* (1972), 10, pp. 1787-1803
[27] Issa, R. I., Solution of the Implicitly Discretized Fluid Flow Equations by Operator-Splitting, *J. Comput.Phys., 62* (1986), 1, pp. 40-65
[28] Chen, J. C., Lin, C. A., Computations of Strongly Swirling Flows with Second-Moment Closures, *International Journal for Numerical Methods in Fluids, 30* (1999), 5, pp. 493-508
[29] Mancenau R., Hanjalić, K., Elliptic Blending Model: A New Near-Wall Reynolds-Stress Turbulence Closure, *Physics of Fluids, 14* (2002), 2, pp. 744-756

Paper submitted: March 15, 2013
Paper revised: March 18, 2013
Paper accepted: May 16, 2013